^{55}Mn(n,α)^{53}Cr and ^{59}Co(n,α) reactions at $E_n = 14.1$ MeV

R. Fischer, G. Traxler, M. Uhl, and H. Vonach

Institut für Radiumforschung und Kernphysik der Österreichischen Akademie der Wissenschaften, 1090 Wien, Austria

P. Maier-Komor

Physik-Department der Technischen Universität München, 8046 Garching, Federal Republic of Germany

The energy and angular distributions of the α particles from the ^{55}Mn(n,$x\alpha$) and ^{59}Co(n,$x\alpha$) reactions for 14.1 MeV incident neutrons were measured by means of a multitelescope system. The results concerning total helium production are in good agreement with existing helium accumulation measurements, whereas the angular distributions reported in the literature for the ^{59}Co(n,α) reaction could not be confirmed. The results are analyzed in the framework of the statistical model of nuclear reactions. Comparison of such calculations with the measured α-emission cross sections allows the extraction of nuclear level densities for ^{52}V and ^{56}Mn, the residual nuclei reached in the reactions studied, in the energy region up to the neutron binding energy, and for ^{55}Mn and ^{59}Co, the residual nuclei reached by neutron emission, for energies around 11 MeV. The level densities derived in this way agree very well with the prediction of the back-shifted Fermi-gas model for the level density parameters of Strohmaier and Uhl. For ^{52}V and ^{56}Mn there is also excellent agreement with the level densities derived from average s-wave neutron resonances. The spin cutoff factors derived from the α-particle angular distributions indicate that there is no reduction of the effective moment of inertia below the rigid body value.

I. INTRODUCTION

In a previous study[1] aimed at both determination of nuclear level densities around $A = 50$—60 and determining the nuclear data for fusion for structural materials, the reactions ^{56}Fe(n,α) and ^{60}Ni(n,α) have been investigated. This program was continued with a study of the ^{55}Mn(n,α) and ^{59}Co(n,α) reactions. These nuclei were selected for the following reasons.

(1) There are no recent measurements of the α-particle energy and angular distributions for these elements; contrary to most other structural materials, Mn and Co were not investigated by the Livermore quadrupole spectrometer.[2] There has been some early nuclear emulsion work[3] on the ^{59}Co(n,α) reaction and also a relatively recent Russian investigation[4] of the α particles from both reactions; however, the former suffers from rather poor statistics and the latter gives no information on the energy distribution of the α particles. Thus a remeasurement seemed appropriate.

(2) In addition, these reactions can be used to determine absolute values of nuclear level densities for ^{52}V, ^{55}Mn, ^{56}Mn, and ^{59}Co, which are especially interesting for several reasons:

(a) Comparison of the level densities of ^{55}Mn and ^{59}Co with the previously[1] determined values for ^{56}Fe and ^{60}Ni allows a sensitive test of the effective pairing energy at the common excitation energy of ~ 11 MeV.

(b) For ^{55}Mn high-quality Ericson fluctuation measurements[5] have provided absolute level densities in the 15—23 MeV range which can be compared to and combined with the value at 11 MeV derivable from the study of the ^{55}Mn(n,α) reaction to give a rather complete description

of the level density of this nucleus over a wide energy range.

(c) For the nuclei ^{52}V and ^{56}Mn average spacings for s-wave neutron resonances (in the systems ^{51}V + n and ^{55}Mn + n) are available[6,7] which can be converted to total level densities if an assumption on the spin distribution is made. For ^{52}V the situation is especially favorable; in this nucleus levels of spin 3 and 4 are populated by s-wave neutron capture from ^{51}V. As these spin values are approximately in the peak of the spin distribution, the value of the total level density is rather insensitive to the assumed value of the spin-cutoff factor, and it is possible to make an independent check of our method of deriving absolute level densities from energy-differential α-emission cross sections.

II. EXPERIMENT AND DATA ANALYSIS

The (n,α) reactions were studied by means of a multitelescope system irradiated by 14.1 MeV neutrons produced in the 250 keV accelerator of the Institut für Radiumforschung und Kernphysik. As both the multitelescope system[8,9] and the procedures used for the analysis of the data and their transformation into double-differential particle emission spectra have been described before,[10] only a few details specific to this experiment are given in the following.

The cobalt target was a metallic foil (purity 99.9) of an average thickness of 2.56 mg/cm^2 as determined by weighing; the manganese foil was produced by evaporation on a 96 mg/cm^2 gold backing. Its average thickness was 2.04 mg/cm^2, also obtained by weighing. The homogeneity of the self-supporting Co target was investigated

by measuring the α-energy loss at six positions. For the Mn target evaporated on Au this was done by cutting the target into 24 pieces and weighing them before and after dissolving the Mn in diluted sulfuric acid. From these measurements the deviations from the average of the target thickness corresponding to the individual telescopes could be determined and corresponding correction factors were applied to the data. Correction factors ranged from 0.96 to 1.07 for Co and from 0.81 to 1.29 for Mn. The accuracy of these correction factors is estimated to be about 3.5%.

In order to further reduce the effect of these inhomogeneities the target was rotated by 180° in the middle of each experiment. In this way any influence of the target inhomogeneities on the forward-backward cross section ratio was eliminated, as were the effects of possible small asymmetries between the two halves of the multiwire counter. The difference between these measurements with differently positioned foils was found to agree with the directly observed thickness variation along the foils.

The results were corrected in the usual way for the energy loss in the targets, that is, all particles were assumed to have lost an energy corresponding to half the target thickness. Each of the above targets was irradiated for about 200 h at a neutron source strength of 8.3×10^9 n/s resulting in neutron fluxes from 4.5×10^5 n/cm^{2}s to 2.0×10^5 n/cm^{2}s.

In order to improve the accuracy of the α-energy calibration, two of the 16 background telescopes were used for an energy calibration during the actual experiments. One of the telescopes (at 24°) was equipped with a melamine target, and observation of the ^{14}N(n,α_0) peak provided a calibration point at about 12 MeV; another one was used to observe 5 MeV α particles from a ^{241}Am source. In this way the α-energy scale could be established to better than 200 keV at 14 MeV and even more accurately at lower energies.

For the determination of the absolute neutron flux the previously described LiI monitor, calibrated via the ^{27}Al(n,α) reaction,[10] was used. In addition, the ^{59}Co$(n,2n)^{58}$Co reaction served as a second independent neutron flux monitor when we placed Co foils at the position of telescope 1. As the cross section for this reaction is well known,[11] and the resulting ^{58}Co activity is sufficiently long lived and well suited for accurate γ counting in our $4\pi\gamma$-detection system,[12] this method also allows for measurements of the time-integrated neutron flux to better $\pm 3\%$. Both methods agreed within this uncertainty.

Data analysis was performed in several steps. First α particles were identified by searching for events located in the appropriate regions of the E-ΔE and E-pulse shape signal planes. Figure 1 shows the result of this first step, the raw α-energy spectra for telescope 1 (22°) and the corresponding background spectrum. Subsequently these raw spectra were corrected for chance coincidences, subtracted from each other, converted to absolute c.m. double differential cross sections, and binned into 1 MeV intervals, as this corresponds approximately to the overall energy resolution of the experiment. The raw energy spectra were also checked for impurity peaks from oxygen or car-
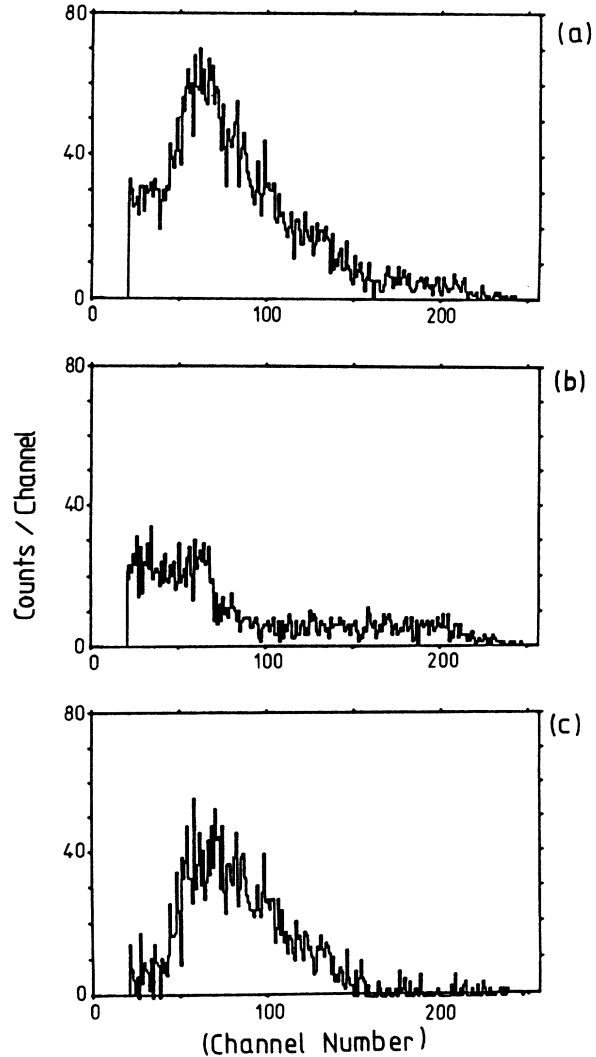
FIG. 1. Raw α-particle spectrum from telescope 1 ($\theta = 22°$). (a) Foreground, (b) background, (c) net α-particle spectrum.

bon. Contrary to our previous ^{50}Cr experiment,[10] no indication for such impurities was found.

III. RESULTS AND DISCUSSION

As the primary result of the data analysis described in Sec. II, double-differential α-emission spectra were obtained for 16 reaction angles ranging from 22° to 165°; the angular resolution of each telescope was on average 13°.[8] Because of the limited statistics of the experiments [total number of true events for Co(n,α), 17.5×10^3, and for Mn(n,α), 7.5×10^3], the individual spectra have rather large statistical errors. Therefore meaningful data were obtained by integrating the results over either energy or angle. Thus we will in the following present and discuss the angle-integrated α spectrum, the α-particle angular distributions for a few rather large α-energy regions, and the total α-emission cross sections.

Table I gives the results for the angle-integrated α-emission cross sections for 1 MeV energy bins which cor-

TABLE I. Angle-integrated α-emission cross section for the reactions ^{55}Mn(n,xα) and ^{59}Co(n,xα) at $E_n = 14.1$ MeV.

E_α (channel energy) (MeV)	$\dfrac{d\sigma}{dE}$ (^{55}Mn + n)^a (mb/MeV)	$\dfrac{d\sigma}{dE}$ (^{59}Co + n)^a (mb/MeV)
4—5	0.61±0.16	0.65±0.14
5—6	1.55±0.17	1.00±0.15
6—7	2.71±0.20	2.77±0.22
7—8	4.74±0.20	6.04±0.34
8—9	4.91±0.18	7.27±0.39
9—10	3.16±0.13	5.74±0.31
10—11	2.00±0.11	4.01±0.23
11—12	1.55±0.09	2.52±0.15
12—13	0.85±0.07	1.35±0.10
13—14	0.56±0.06	1.01±0.08
14—15	0.07±0.04	0.36±0.04

^{a}Correlated part of the uncertainties 3.5%.

respond roughly to the energy resolution of the experiments. The errors given are effective 1σ errors obtained by adding the statistical errors and estimates of all identified sources of systematic error in quadrature. Systematic errors are included for uncertainties in neutron flux (3%), effective target thickness (3%), solid angle of telescopes (1.7%), dead time correction (1%), and the uncertainties in the boundaries chosen for particle identification in the E-ΔE and E-pulse shape planes (see Ref. 9).

For the ^{55}Mn(n,xα) reaction no previous measurements of the α spectrum exist. For the ^{59}Co(n,α) reaction our results can be compared to the (un-normalized) α spectrum given in Fig. 3 of Ref. 3; however, it has to be kept in mind that there the α spectrum is given in terms of c.m. α energy that differs from channel energy by $\sim 7\%$. If this is taken into account there is agreement within errors.

The total α-emission cross sections obtained by numerical integration of the $d\sigma/dE_\alpha$ values are given in Table II, where they are compared with the results of Ref. 3, with helium production cross sections,[13] and with activation cross sections for the ^{55}Mn(n,α)^{52}V and ^{59}Co(n,α)^{56}Mn reactions taken from the recent evaluation of Smith[14] which gives a weighted average of all measurements before 1983. For the ^{55}Mn(n,α) reaction, in addition the results of a recent precise activation measurement,[15] not included in Ref. 14, are also given. For Co our results agree within error both with α-emission cross

sections of Ref. 4, the helium accumulation measurement, and the activation cross sections, if it is taken into account that the α-emission cross section is expected to increase by $\sim 10\%$ between 14.1 and 14.8 MeV and that the activation cross section at 14.7 MeV should be about 20% lower than the α-emission cross section because this fraction of the α spectrum is below the ^{59}Co(n,nα) threshold. For Mn our total α-emission cross section is roughly in agreement with the results of helium accumulation measurements[13] if the expected increase in helium production between 14.1 and 14.8 MeV ($\sim 13\%$) is taken into account. It is, however, definitely lower than both the value of Ref. 3 and the activation cross section derived in Ref. 14. This cannot be explained by the already mentioned change of the α-emission cross section with neutron energy or the Mn(n,αn) cross section, which is negligible because of its more negative Q value.

Concerning Ref. 4, it has to be noted that there are problems with absolute cross section values for some cases like the ^{51}V(n,xα) cross section, which is too high; thus a similar situation might exist for ^{55}Mn. Concerning the activation cross sections, a closer look at the data used in Ref. 14 shows that there are essentially two groups of results clustered around 27 and 33 mb, respectively, and the evaluated value lies in the middle between the two groups. However, the recent additional measurement definitely supports the lower cross section values. Thus it seems probable that the true ^{55}Mn(n,α)^{52}V activation cross section is closer to the value of Ref. 15 than to Ref. 14 and is thus in agreement with out total α-emission cross section.

Figures 2 and 3 show the angular distributions obtained for different α-energy regions. In these figures the data points are given with their uncorrelated errors only. The figures show that there are considerable contributions from noncompound reactions at the highest α energies, probably due to direct excitations populating low lying levels as already observed for ^{50}Cr, ^{56}Fe, and ^{60}Ni.[1,10] In the region of the evaporation maximum [see Figs. 2(a) and 3(a)] the angular distributions are approximately symmetric around 90°, as expected according to the Hauser-Feshbach (HF) theory. The size of the cross section at 90° minimum is about the same as in our earlier measurements on ^{50}Cr, ^{56}Fe, and ^{60}Ni. For Mn the shape of the overall angular distribution agrees well with the results of Ref. 4 (although there is a discrepancy in the absolute cross section values as discussed before), whereas for Co Ref. 4 reports a very different angular distribution with a deep minimum at 90°,

TABLE II. Total α emission and helium production cross section (CS) for the reactions ^{55}Mn(n,xα) and ^{59}Co(n,xα) and activation cross section for the ^{55}Mn(n,α) and ^{59}Co(n,α)^{56}Mn reactions.

E_n (MeV)	σ (^{55}Mn) (mb)	σ (^{59}Co) (mb)	Type of CS	Ref.
14.1	22.7±1.2	32.8±1.6	α emission	This work
14.7	36.9±5.2	39.9±6.2	α emission	4
14.8	28±2	40±3	helium production	13
14.7	31.2±3.8	30.2±1.8	activation	14
14.7	23.2±0.7	30.2±1.5	activation	15
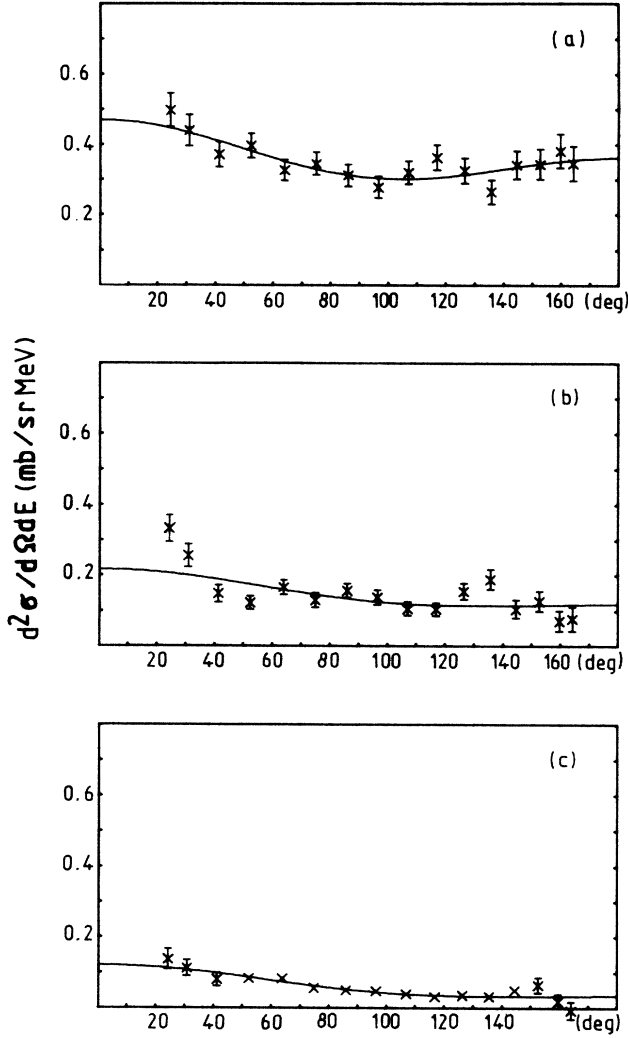
FIG. 2. Angular distributions for different α-energy bins for the ^{55}Mn(n,α) reaction. (a) $E_{\alpha ch} = 7-10$ MeV, (b) $E_{\alpha ch} = 10-12$ MeV, (c) $E_{\alpha ch} = 12-14$ MeV. The solid curves denote Legendre fits to the data. (Experimental errors are shown only if larger than the size of the symbols.)

$$\left[\frac{d\sigma}{d\Omega} \right]_{90°} \bigg/ \left[\frac{d\sigma}{d\Omega} \right]_{0° \text{ or } 180°} \sim 0.4 \ .$$

Such a difference between the α-particle angular distributions for reactions on rather similar nuclei seems unlikely; thus it appears to us that the Co(n,α) results of Ref. 4 might be influenced by some unidentified experimental problems. The same applies, although to a somewhat lesser extent, to the angular distribution reported in Ref. 3.

IV. DETERMINATION OF NUCLEAR LEVEL DENSITIES AND SPIN-CUTOFF FACTORS

The measured α-particle spectra were used to derive absolute values of the nuclear level densities for the residual nuclei reached by α emission, ^{52}V and ^{56}Mn, for excitation

energies between the region of resolved levels and the neutron binding energy and the level densities of the target nuclei ^{55}Mn and ^{59}Co at an excitation energy of ~ 11 MeV. In addition, the angular distributions in the evaporation peak [see Figs. 1 and 2(a)] were used to derive values for the spin-cutoff factor σ used.

The method for deriving absolute level densities from angle-integrated particle emission in compound nucleus reactions and for estimating the uncertainty of the level density values has been described in detail before;[1,16] therefore we will only mention principles of the method and some points specific to the analysis of the data of this experiment and then present the results. The extraction of the total level densities summed over all spin and parity values was done in the following way.

(1) The angle integrated α-particle emission cross sections were calculated within the Hauser-Feshbach formalism using the code STAPRE (Ref. 17) using a set of parameters (transmission coefficients and level density parameters) which had previously been derived in an overall evaluation of neutron cross sections for structural materials.[18]

(2) The results of this calculation are compared to the α-emission cross section measurements in the region of resolved levels. In this region, the cross sections are essentially determined by the ratio of the decay widths to these levels to the total decay width of the compound nuclei, which is dominated by the neutron width and thus by the level density of the nuclei reached by neutron emission (= target nucleus) in the excitation energy range populated in the evaporation process. Therefore, the level density parameters of this residual nucleus are slightly varied until agreement with the measured α-emission cross section in the region of resolved levels is obtained. In this way we determine the level densities of the target nuclei at an excitation energy $U \sim E_0 - 2T$ (E_0 is the incident neutron energy, T is the nuclear temperature at E_0) (Ref. 16) which amounts to $U \sim 11$ MeV in our cases.

(3) Having fixed the level densities of the residual nuclei reached by neutron and proton emission in the described way, we repeat the calculation of the α-emission cross sections and get the level densities for the residual nucleus reached by α emission by means of the relation

$$\rho(U) = \rho(U)_{\text{assumed}} \left[\frac{\left[\dfrac{d\sigma}{dE_\alpha} \right]_{\text{meas}}}{\left[\dfrac{d\sigma}{dE_\alpha} \right]_{\text{calc}}} \right]_{E_\alpha = E_{\alpha \max} - U} ,$$

where $\rho(U)$ is the total level density of the residual nucleus according to the α-emission cross section $(d\sigma/dE_\alpha)_{\text{meas}}$ and $\rho(U)_{\text{assumed}}$ is the total level density of the residual nucleus assumed in the calculation of $(d\sigma/dE_\alpha)_{\text{calc}}$; E_α is the channel energy for α-particle emission.

In applying this method to the present experimental results we used the excitation energy regions $U = 0-2.3$ MeV ($E_{\alpha ch} = 11-13.3$ MeV) for ^{52}V and $U = 0-1.8$ MeV ($E_{\alpha ch} = 12.5-14.3$ MeV) as regions of known discrete levels for step (2). The whole analysis was done as

TABLE III. Approximate ratio of $(d\sigma/d\Omega)_b/(d\sigma/d\Omega)_0$ for particle emission into the backward hemisphere to forward emission for direct and precompound reactions. [$(d\sigma/d\Omega)_b$ =average value of differential particle emission cross section for $\theta = 90°-180°$.]

Reaction	Outgoing particle energy (MeV)	$\left[\dfrac{d\sigma}{d\Omega}\right]_b / \left[\dfrac{d\sigma}{d\Omega}\right]_0$	Ref.
^{93}Nb(n,$x\alpha$)	14—16	~0.1	19
^{93}Nb(n,p)	12—14	~0.15	20
^{54}Cr(p,α_0)	15.1—15.8	~0.12	5
systematic derived from many expt. data	12—14	~0.15	21

described in Refs. 1 and 14 with one modification concerning the correction for noncompound contributions to the measured α-emission spectra.

As is obvious from the angular distributions in Figs. 2 and 3, the high energy parts of the α spectra, which feed the region of discrete levels, do contain a sizable contam-

ination by direct and/or precompound reactions. In Ref. 1 we therefore only used the experimental spectrum integrated over the backward hemisphere (90°—180°) for the comparison with the HF calculations; we made, however, no correction for the certainly existing noncompound emission into the backward hemisphere, but considered this effect only in the error analysis by an additional term.

Such procedures, which use a purely one-sided uncertainty, should in principle be avoided, as they introduce a
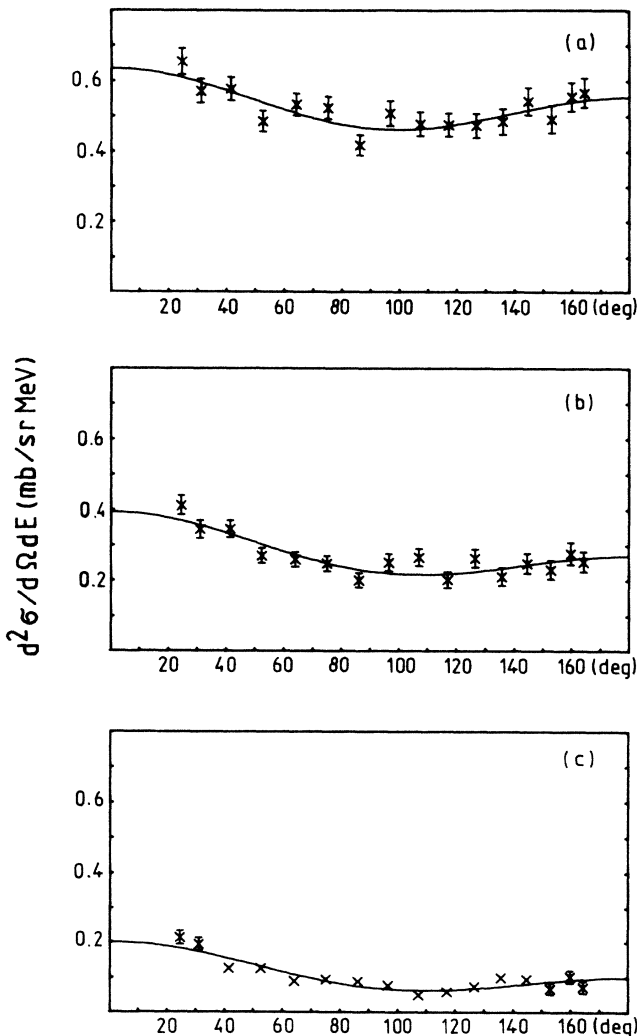
FIG. 3. Angular distributions for different α-energy bins for the ^{59}Co(n,α) reaction. (a) $E_{\alpha\text{ch}}=7-10$ MeV, (b) $E_{\alpha\text{ch}}=10-12$ MeV, (c) $E_{\alpha\text{ch}}=12-14$ MeV. The solid curves denote the Legendre fits to the data.
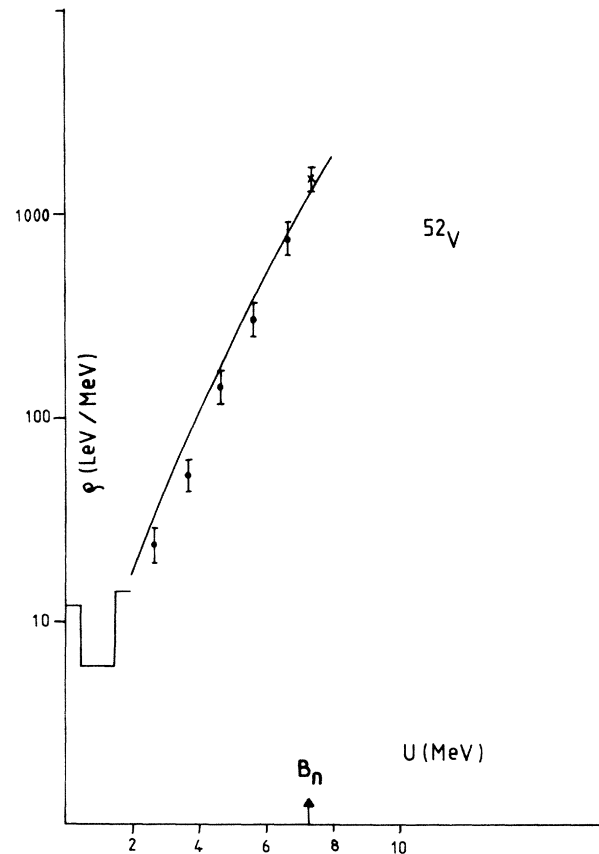
FIG. 4. Level density of ^{52}V. The histogram is derived from the counting of discrete levels; ● denotes the level density from $d\sigma/dE_\alpha$ values; × denotes the level density derived from s-wave neutron resonance spacing assuming a rigid body moment of inertia ($\sigma=3.96$); — denotes the back-shifted Fermi-gas model with $a=6.16$ MeV^{-1} and $\Delta=-1.46$ MeV (Ref. 18).
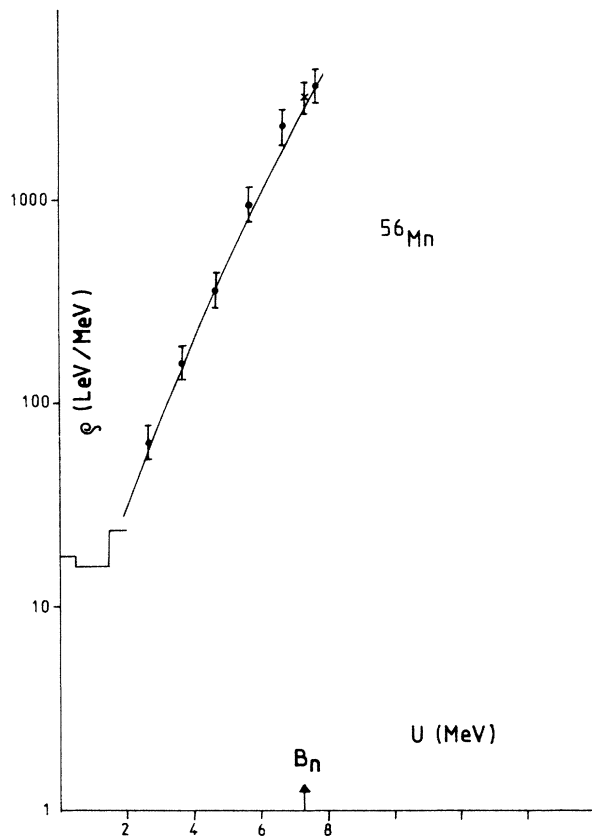
FIG. 5. Level density of ^{56}Mn. $\times$ denotes level density derived from s-wave neutron resonance spacing assuming a rigid body moment of inertia $(\sigma = 4.1)$; — denotes the Fermi-gas model with $a = 6.81$ MeV^{-1} and $\Delta = -1.5$ MeV (Ref. 18). Other symbols are as in Fig. 3.

FIG. 6. Level density of ^{55}Mn. The histogram is derived from counting of discrete levels; $\bigcirc$ denotes the level density derived from α-emission cross sections into the region of resolved levels; $\triangle$ denotes level densities from Ericson fluctuations (values of Ref. 5 corrected as described in the text). Solid line: Fermi-gas model with $a = 6.25$ MeV^{-1}, $\Delta = -0.7$ MeV. Dashed line: constant temperature model with $T = 1.6$ MeV.

bias into the analysis. Therefore in this analysis we will derive an estimate for the noncompound contribution to the α spectra in the backward hemisphere from the measured angular distributions and subtract this estimate from the measured $d\sigma/dE_\alpha$ values before the comparison with the HF calculations is done. For this purpose we need the angular distribution of noncompound α particles of energies 12–14 MeV. On this question we do have some information which is summarized in Table III.

From this roughly consistent information given in Table III we assume a value of 0.12 ± 0.06 for the ratio

$$\left[\left[\frac{d\sigma}{d\Omega}\right]_b \Bigg/ \left[\frac{d\sigma}{d\Omega}\right]_{0^\circ}\right]_{\text{noncomp}}$$

Accordingly our experimental $(d\sigma/dE_\alpha)$ values are corrected by a correction factor f_{noncomp} given by

$$f_{\text{noncomp}} = 1 - \frac{0.12}{1 - 0.12} \frac{\left[\dfrac{d\sigma}{d\Omega}\right]_0 - \left[\dfrac{d\sigma}{d\Omega}\right]_b}{\left[\dfrac{d\sigma}{d\Omega}\right]_b}$$

An uncertainty of $\sim 50\%$ for $1 - f_{\text{noncomp}}$ is assumed. In our cases the correction factor amounted to 0.86 for ^{55}Mn

TABLE IV. Measured and calculated nuclear level densities at $U = 11$ MeV.

Nucleus (MeV)	ρ_{exp} (level density/MeV)	ρ_{Dilg} (level density/MeV)	$\rho_{\text{Strohmaier-Uhl}}$ (level density/MeV)	T_{exp} $(U = 3-11)$ (MeV)
^{55}Mn	$6.4 \times 10^3 \pm 25\%$	8.2×10^3	5.6×10^3	1.55 ± 0.07
^{56}Fe	$3.05 \times 10^3 \pm 25\%$	2.9×10^3	3.4×10^3	1.41 ± 0.07
^{59}Co	$17.4 \times 10^3 \pm 25\%$	10.25×10^3	18.3×10^3	1.26 ± 0.07
^{60}Ni	$3.85 \times 10^3 \pm 25\%$	3.6×10^3	6.0×10^3	1.39 ± 0.07

and 0.78 for ^{59}Co.

The level densities of ^{52}V and ^{56}Mn derived in this way, the level densities derived from counting of discrete levels and the values obtained from the density of s-wave resonances[6,7] assuming spin cutoff factors (4.0 for ^{52}V and 4.1 for ^{56}Mn) corresponding to a rigid body value for the effective nuclear moment of inertia, are shown in Figs. 4 and 5. The given uncertainty for the level density value derived from neutron resonance spacings includes both the experimental error in the measurements of the average resonance spacings and an assumed uncertainty of 30% in the effective nuclear moment of inertia. Due to the particular values of the target spin ($\frac{5}{2}^-$ and $\frac{7}{2}^-$), the dependence of the total level densities on the assumed spin cutoff factors is relatively weak, and thus for these nuclei it is possible to derive rather accurate total level densities (see Figs. 4 and 5) from the observed average s-wave neutron resonance spacings in spite of the rather large uncertainty about the effective nuclear moment of inertia. As the figures show, there is excellent agreement between the total level density derived from neutron resonances and the value obtained from our statistical model analysis of the α-emission spectra which gives an additional independent check for our procedure, especially the estimates used to correct for noncompound reactions.

The absolute level density values derived from the α-emission cross sections are also in agreement with the predictions of the back-shifted Fermi-gas model with parameters by Strohmaier and Uhl[18] for the mass region $A = 50-60$ (solid lines in Figs. 3 and 4).

Figure 6 shows the level density values for ^{55}Mn at 11 MeV derived from the α-emission cross section into the region of discrete levels, and the level density values from counting of discrete levels and those from Ericson fluctuations.[5] The level densities reported in Ref. 4 have been derived from a statistical model analysis of fluctuation measurements of the ^{54}Cr(p,α) reaction. In this analysis the Huizenga-Igo potential[22] was used for the α-transmission coefficients. It was later shown[23] that this potential is inadequate at low α-particle energies and should be replaced by more appropriate parametrizations. Therefore we reanalyzed the data of Ref. 5 using the α-particle potential of Satchler-McFadden[24] which especially reduced the level density value at the lowest excitation (from 1.1×10^5 to 6.8×10^4 MeV^{-1}).

As the figure shows, there seems to be an almost purely

TABLE V. Spin-cutoff factors derived from α-particle angular distribution.

Nucleus	Excitation energy (MeV)	σ	I/I_{rigid} ($r_0 = 1.25$ fm)
^{52}V	3.3—6.3	$3.22^{+1.90}_{-0.54}$	0.75
^{56}Mn	4.2—7.2	$3.54^{+1.14}_{-0.47}$	0.80

exponential increase of the level density of ^{55}Mn for excitation energies up to 24 MeV characterized by a nuclear temperature of about 1.6 MeV, whereas the functional form of the Fermi-gas model does not fit the data as well. This behavior is rather different from our previous results on ^{56}Fe and ^{60}Ni, which definitely favor the Fermi-gas model, as is also expected theoretically.

Finally, all our level density results at $U = 11$ MeV are summarized in Table IV (the values for ^{56}Fe and ^{60}Ni taken from Ref. 1 have been corrected for noncompound contributions too) and compared to the predictions of the back-shifted Fermi-gas model using either the parameters of Dilg et al.[25] [Eq. (10) of Ref. 23] or those of Strohmaier and Uhl.[18] In addition, the average nuclear temperatures in the excitation energy range 3—11 MeV derived from the experimental level density values of 11 MeV and the density of discrete levels around 3 MeV are also given. As the table shows, there is rather good agreement with the level density parameters derived by Strohmaier and Uhl[18] from a simultaneous evaluation of neutron cross sections of structural materials, whereas the global parameters of Dilg et al.[25] for the $A = 40-65$ mass range predict level densities which may deviate somewhat more from the experimental values, at least for the case of ^{59}Co.

Spin-cutoff factors were determined from comparison of the α-particle angular distributions in the region of the evaporation peak with statistical model calculations. The resulting values are given in Table V. As in all our previous studies,[1,10] the spin-cutoff factors are consistent with an effective nuclear moment of inertia equal to the rigid body value.

[1]R. Fischer, G. Traxler, M. Uhl, and H. Vonach, Phys. Rev. C 30, 72 (1984).

[2]K. R. Alvar et al., Nucl. Instrum. Methods 148, 303 (1978).

[3]W. Patzak and H. Vonach, Nucl. Phys. 39, 263 (1962).

[4]G. P. Dolya et al., Kiev Report 1977, Vol. 2, p. 68; Institution Ukrainsk Fiz. Tekhn. Inst. Kharkov Report KFTI 76-50, 1976.

[5]A. A. Katsanos et al., Phys. Rev. C 1, 594 (1970).

[6]J. Gary, R. L. Macklin, and J. Halperin, Phys. Rev. C 18, 2079 (1978).

[7]R. R. Winters, R. L. Macklin, and J. Halperin, Phys. Rev. C 18, 2092 (1978).

[8]C. Derndorfer et al., Nucl. Instrum. Methods 187, 423 (1981).

[9]G. Traxler, R. Fischer, and H. Vonach, Nucl. Instrum. Methods 217, 121 (1983).

[10]C. Derndorfer, R. Fischer, P. Hille, and H. Vonach, Z. Phys. A 301, 327 (1981).

[11]S. J. Hasan, A. Pavlik, G. Winkler, and M. Kaba, in Proceedings of the International Conference on Nuclear Data for Basic and Applied Science, 1985, Santa Fé, New Mexico (in press).

[12]A. Pavlik and G. Winkler, Int. J. Appl. Radiat. Isot. 34, 1167 (1983).

[13]D. W. Kneff et al., Nucl. Sci. Eng. 92, 491 (1986).

[14]B. P. Evain, D. L. Smith, and Paul Lucchese, Argonne National Laboratory Report ANL-NDM-89, 1984.

[15]R. Pepelnik *et al.*, Nuclear Energy Agency Nuclear Data Committee Report NEANDC(E) 252 U, 1984.

[16]H. Vonach, in Proceedings of the Advisory Group Meeting on Basic and Applied Problems of Nuclear Level Densities, Brookhaven National Laboratory Report BNL-NCS 51594, 1983, p. 247.

[17]M. Uhl, IAEA Report 190, 1976, p. 361.

[18]B. Strohmaier and M. Uhl, in *Proceedings of the International Conference for Science and Technology, Antwerp, 1982* (Reidel, Dordrecht, 1983), p. 361.

[19]R. Fischer, C. Derndorfer, B. Strohmaier, and H. Vonach, Ann. Nucl. Energy **9**, 409 (1982).

[20]G. Traxler *et al.*, Nucl. Sci. Eng. **90**, 174 (1985).

[21]C. Kalbach and F. Mann, Phys. Rev. C **23**, 112 (1981).

[22]J. R. Huizenga and G. R. Igo, Argonne National Laboratory Report ANL-6373, 1961; Nucl. Phys. **29**, 462 (1962).

[23]H. Vonach, R. C. Haight, and G. Winkler, Phys. Rev. C **28**, 2278 (1983).

[24]L. McFadden and G. R. Satchler, Nucl. Phys. **84**, 177 (1966).

[25]W. Dilg, W. Schantl, H. Vonach, and M. Uhl, Nucl. Phys. **A217**, 269 (1973).